



# Treatment Planning Considerations for Prostate SBRT and MRI Based Planning **2**

Neelam Tyagi and Margie Hunt

## 2.1 Introduction

Without question, external beam radiotherapy for prostate cancer is in a period of rapid change and evolution. The radiotherapy community is witnessing a paradigm shift from conventional fractionation schemes with doses as high as 80–86 Gy and durations up to 9 weeks to hypofractionated approaches incorporating moderate (~2.5–4 Gy/fraction) to extreme (~6.5–9 Gy/fraction) fractionation [1–11]. Such techniques are gaining acceptance as being comparable to conventional fractionation both in terms of tumor control and toxicity. Furthermore, multiple trials are underway to determine the feasibility and efficacy of boosting dominant intra-prostatic lesions (DIL) using simultaneous integrated boost (SIB) techniques [12–16]. From a clinical standpoint, hypofractionated radiotherapy methods are an outgrowth of both the favorable radiobiological characteristics of prostate cancer [17–20] and patient convenience. However, without doubt, technological advances including image guided radiotherapy (IGRT) [21, 22], volume modulated arc therapy (VMAT) [23–26], magnetic resonance imaging (MRI) for segmentation and planning [27–30], and anatomic modulators such as bio-absorbable

injectable rectal spacers [31–34] are what has made prostate hypofractionated treatment possible.

Of particular importance is the role of MRI in the simulation and planning for prostate stereotactic body radiotherapy (SBRT). Although CT has been the mainstay of radiotherapy planning for nearly 40 years and will likely continue as such for the near future, the superiority of MRI's soft tissue contrast for target and normal tissue segmentation has been appreciated for some time. Multiple studies have demonstrated the value of MRI to visualize the prostate gland and dominant lesions for external beam radiotherapy planning [35–37]. Furthermore, many groups have shown that CT-based segmentations of the prostate are consistently larger (up to 30–40%) than those from MRI [38–40]. The smaller MR-based segmentations result from improved visualization of the prostatic apex and base as well as the tissue planes differentiating the prostate from surrounding soft tissues. Although a strong argument can therefore be made that incorporating MRI decreases over-segmentation of the prostate, a wider transition to combined CT-MRI methods has been hampered by concerns about segmentation errors introduced by mis-registration of the image sets and the changes to the shape and location of the soft tissues (e.g. bladder, rectum, seminal vesicles) inherent when acquiring multiple image sets. Furthermore, scanner-induced distortions of the MR

---

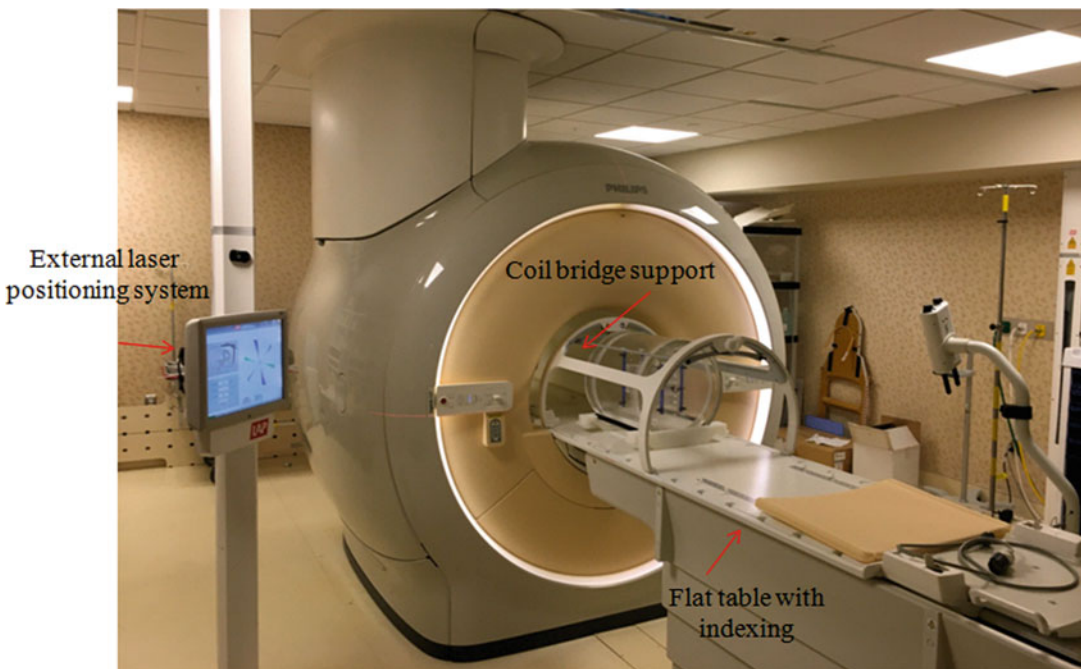
N. Tyagi (✉) · M. Hunt  
Department of Medical Physics, Memorial Sloan  
Kettering Cancer Center, New York, NY, USA  
e-mail: tyagin@mskcc.org; huntm@mskcc.org

images have led to concerns about the geometric fidelity of the images and its subsequent impact on target localization.

Fortunately, recent advances in MR scanner hardware and software are addressing most of these concerns. With modern scanners, geometric distortions are relatively small and can be sufficiently characterized so as to be manageable for many radiotherapy patients, including those undergoing prostate radiotherapy [41]. Even more significantly, recent improvements have led to the commercial availability of MR-based and MR-only simulation systems [41–44]. Similar to CT simulators, MR simulators include flat tabletops with indexing, external laser positioning systems (ELPS), MR-compatible immobilization and radiotherapy specific scanning protocols. Figure 2.1 shows an example MR simulator along with the radiotherapy-specific components.

Another crucial requirement for MR-only simulation and planning for prostate radiotherapy that has only recently become commercially available is the so-called “synthetic-CT” or

“pseudo-CT”. A synthetic CT image is one created directly from an underlying base MR image using some method of tissue segmentation or classification and subsequent assignment of a CT or Hounsfield number which describes, with sufficient accuracy, the x-ray attenuation properties of the tissue. Generation of synthetic CT images has been an area of active research for many years, however recent progress has been spurred by the development of combined positron emission tomography (PET)/MR scanners for which a synthetic CT must provide the attenuation correction information required for accurate PET assessment. Synthetic CT images are, of course, also essential for MR-only planning because they provide electron density information for accurate dose calculation. Synthetic CT generation approaches can be broadly categorized into those that assign bulk electron densities to structures either manually segmented or obtained from multiple MR sequences to classify tissue types [45, 46] and those that use a patient atlas of paired CT and MR images and deformable



**Fig. 2.1** MR simulator illustrating some of the radiotherapy-specific components such as external laser positioning system, flat table top with indexing and a coil bridge support

registration to assign CT numbers on a voxel-by-voxel basis to the MR image of a new patient [47, 48].

It is hopefully apparent that as a result of the advances described above, the radiotherapy community is now poised to transition to an era where MRI becomes the predominant imaging modality for segmentation and planning of prostate cancer. With this in mind, this chapter will focus on immobilization, simulation and planning for prostate SBRT, with an emphasis on MR-based techniques. Collectively with Chap. 5 (segmentation) and Chap. 4 (image-guided treatment delivery and motion management), the technical components of a SBRT prostate radiotherapy program are fully described. As with all radiotherapy, variations to the techniques described herein can be successfully applied and therefore, as appropriate, references to other methods are provided. The reader is also referred to the article by Clemente et al. [49] which provides a fairly comprehensive review of technical approaches for moderate and extreme hypofractionated prostate radiotherapy. When implementing SBRT for prostate cancer, it is important to remember that it is the cumulative effect of all aspects of the technical program that impacts the success of the clinical program. Therefore, the synergies and dependencies of different technical components (e.g. uncertainty in treatment delivery and margin definition) must be carefully considered and evaluated within the context of the entire program.

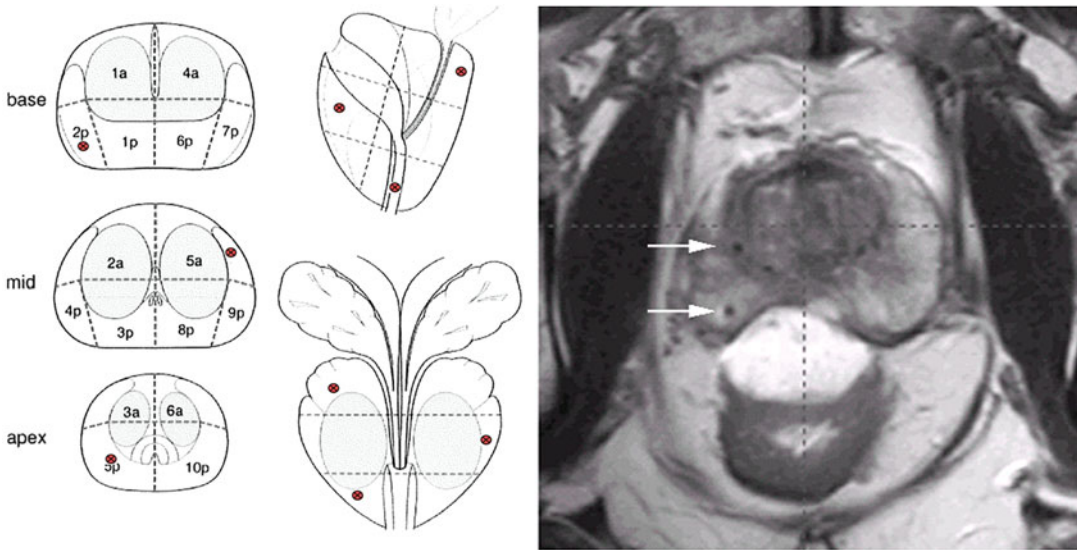
---

## 2.2 Simulation and Image Acquisition

Particularly with hypofractionated SBRT treatment paradigms, consistency and adherence to procedures for pre-simulation activities, immobilization, and the acquisition of images is crucial so that the conditions necessary for successful treatment can be created at the time of simulation and reproduced at each treatment to the greatest degree possible.

### 2.2.1 Pre-Simulation Considerations

The selection of a method to position and track prostate motion during treatment delivery is an important decision made prior to radiotherapy simulation since it may require the implantation of fiducials into the prostate gland. Implanted electromagnetic beacons [50–52] are incompatible with MR imaging for simulation and planning due to the creation of image artifacts and therefore, another method, such as implantation of gold seed fiducials, to aid image-based setup [53, 54] or track prostate motion during treatment [55] may be needed. In that case, preparation for SBRT radiotherapy may begin several weeks prior to simulation with the placement of three radio-opaque gold fiducial seeds (typically 3–5 mm in length and 0.9–1.2 mm in diameter) distributed evenly throughout the prostate (Fig. 2.2). Furthermore, the insertion of an anatomic modulator in the form of an injectable rectal hydrogel spacer [31, 32, 34, 56–58] should be considered to create distance between the anterior rectum and the prostate and reduce the rectal volume irradiated to the intermediate and high dose levels. Although additional outcome data are still needed, the use of a rectal spacer may significantly reduce the likelihood of high grade and acute rectal toxicity. A multi-institutional clinical trial [33] found that the injection of hydrogel into the prostate-rectal interface resulted in rectal dose reduction in more than 90% of patients. These results were observed even in the presence of significant variability in planning approaches and injection results across participating institutions. An analysis of the 12 month toxicity from this same trial [34] revealed a Grade 1 late GI toxicity rate of only 4.3%, no late Grade 2 or higher GI toxicity, and no evidence of ulceration, stricture or necrosis. The authors concluded that the use of the spacer was a safe and effective method for sparing the rectum from high radiation dose. Figure 2.2 demonstrates typical placement of a bio-absorbable gel to create a space of approximately 1 cm between the prostate and anterior



**Fig. 2.2** (Left panel) Suggested placement of gold seed fiducials (red circles) within the prostate to ensure optimal visualization for pre- and intra-treatment image-guided radiotherapy. Courtesy of Tomer Charas, M.D. (Right

panel) Representative T2-weighted MR image demonstrating both a bio-absorbable gel within the recto-prostatic interstitial space and gold seed fiducials (arrows)

rectal wall. When technically feasible, spacer placement can be offered to eligible patients at the same time as gold seed fiducial placement. The gel remains in the body for about 12 weeks which is sufficient time for SBRT simulation, planning and treatment, after which hydrolysis liquefies the implant, resulting in complete absorption.

Patient bowel and bladder preparation prior to simulation is an additional crucial first step in ensuring accurate planning and treatment delivery. At Memorial Sloan Kettering Cancer Center (MSKCC), the goal is reproducible filling at simulation and each treatment session with the rectum being as close to empty as possible and the bladder being tolerably full. The standard pre-simulation preparation includes a bowel preparation of Metamucil<sup>®1</sup> (1 Tbsp/8 oz) for 7 days prior to simulation, Fleet<sup>®2</sup> enema 3 h before simulation, and optional Gas-X<sup>®3</sup> (two tablets the night before and the morning of simulation).

On the day of simulation, an initial evaluation of bowel evacuation is performed using a small number of CT or MR images. A rectal catheter is inserted to remove rectal gas if necessary. All SBRT patients are simulated and treated with a full bladder obtained by asking the patients to first void and then to drink one cup of water 45 min prior to their planned procedure. Patients continue with the Metamucil<sup>®</sup>, Fleet<sup>®</sup> enema and optional Gas-X<sup>®</sup>, as described above, daily throughout their course of SBRT.

### 2.2.2 Immobilization

Immobilization is another important step in the SBRT treatment planning process. With the advent of image-guided radiotherapy however, the focus of immobilization has been directed more toward daily setup reproducibility and management of motion during treatment than on rigid immobilization to ensure accurate set-up based on skin marks at the start of the treatment session. Historically, several immobilization approaches have been successfully used for prostate cancer including thermoplastic molds and foam or

<sup>1</sup> Procter & Gamble Company, Cincinnati, OH 45202.

<sup>2</sup> C.B. Fleet Company, Lynchburg, VA 24502.

<sup>3</sup> GlaxoSmithKline, Warren, NJ 07059.

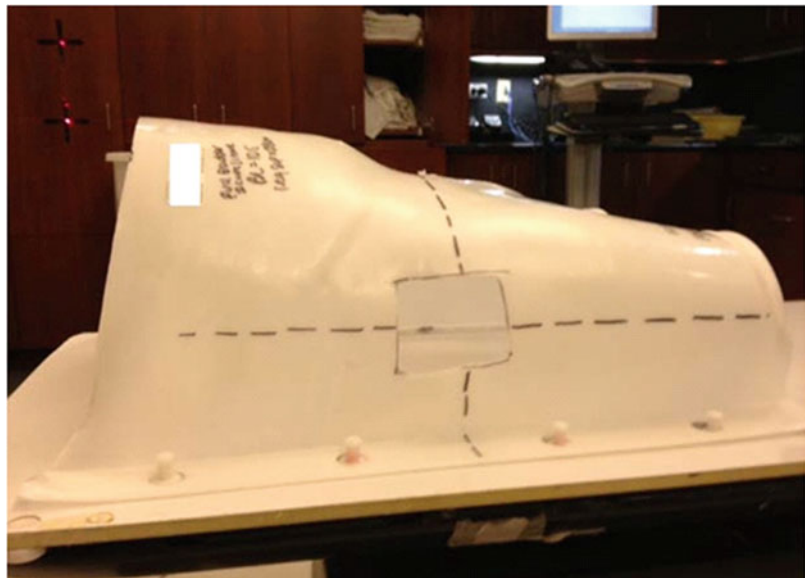
vacuum bag body cradles [49]. These devices help to ensure reproducible initial positioning of the patient. Subsequently, daily image guidance (e.g. orthogonal kV radiographs and/or cone beam CT) must be used to ensure that the position of the prostate with respect to the isocenter is also accurate and within acceptable levels determined by the uncertainty of the image registration method [54, 59]. Without such a process, Algan et al. [60] demonstrated that the dosimetric impact could be underdosing of the prostate gland by 7% or more for conventional fractionation schemes and prostate margins of 5–7 mm (3–5 mm posteriorly).

At MSKCC, patients are simulated in a head first, supine position using a simple, flat custom-built board that can be indexed to the couch top and an anterior solid thermoplastic mold that extends from approximately mid-abdomen to mid-thigh (Fig. 2.3). The mold closely conforms to the contours of the inner leg and a knee cushion is standardly used to provide additional stability. Such an approach may potentially provide an improved rectum-prostate configuration [61].

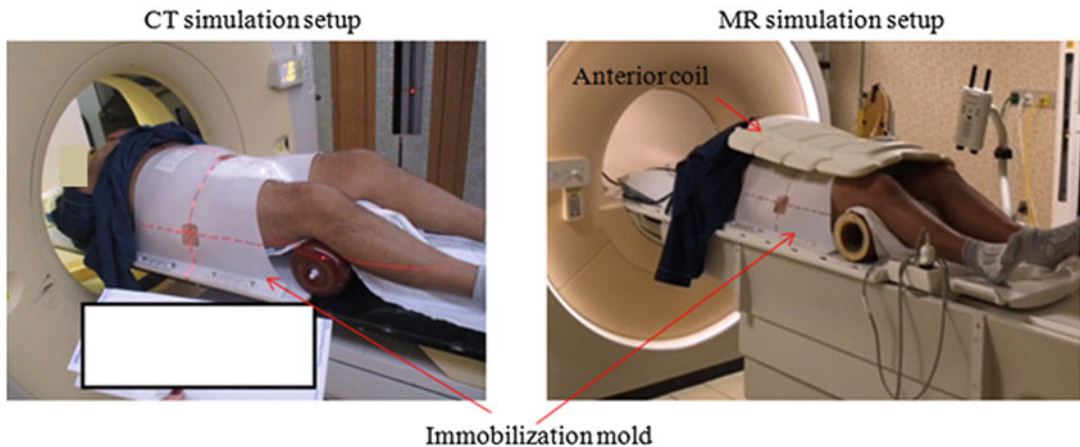
### 2.2.3 Simulation Workflow 1: Primary CT Simulation with Secondary MR Imaging and Fusion

In this workflow, CT images are acquired from L1 to well below the ischial tuberosities and reconstructed at no more than a 2 mm slice thickness. Just prior to simulation, a Foley catheter is inserted to facilitate visualization and segmentation of the urethra. CT simulation is then followed by an MR session with the patient placed in his immobilization mold with an indexed flat tabletop, and initially positioned using ELPS. Anterior and posterior radiofrequency (RF) coils are both used for imaging. Particularly if the patient is immobilized with an open body mold, a coil bridge should be used so the patient's anatomy is not distorted by the anterior coil. Failure to do so has been associated with deformation of the anterior skin surface by up to 1.7 cm [62]. If, on the other hand, a sufficiently rigid immobilization mask is used (Fig. 2.3), the anterior coil can be placed directly on the immobilization mold itself with the added advantage of minimizing the distance between the coil and patient surface. If the MR scanner is equipped with a built-in posterior

**Fig. 2.3** Solid thermoplastic mold for SBRT prostate radiotherapy with cutouts for laser-based triangulation positioning







**Fig. 2.4** Simulation setup in the CT and MR scanners for a multi-modality simulation workflow

spine coil, care must also be taken to use a flat table top that minimizes the distance between the coil and patient. Some newer scanners provide an option for a flat table that does not add distance between the patient and coil. Such a table serves as a replacement for the standard curved diagnostic table and is preferred to a curved table with a flat table top add-on.


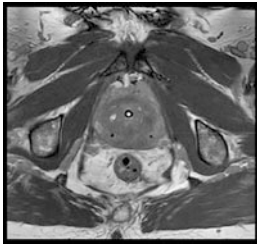
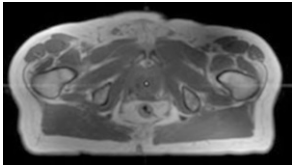
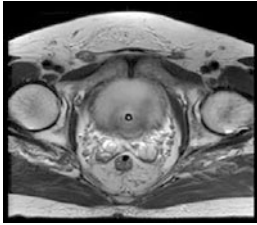
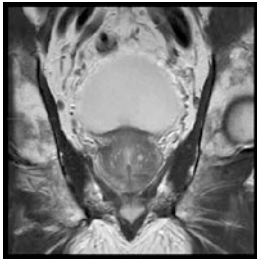
Patient positioning should be as close as possible for both the CT and MR imaging sessions. Registration inaccuracies of more than 2 mm have been reported when MR images acquired with the patient in the diagnostic position are used for planning [63] and such a workflow is not recommended for SBRT planning. For a combined CT and MR simulation workflow, registration uncertainty can be further minimized by keeping the time between the CT and MR sessions as short as possible, thereby maximizing consistency of the bladder and rectal contents. If the patient must void between sessions or is otherwise unable to complete both CT and MRI on the same day, an attempt must be made to ensure consistent rectal and bladder filling for both imaging procedures. To further reduce inaccuracies and improve the MR simulation, Foley catheter usage during CT and MRI should also be consistent and glucagon administration during the MRI can be considered to minimize peristalsis and the associated motion artifacts. Prior to placing the

custom immobilization device on the patient during the MRI session, it is often helpful to first set the patient up using the ELPS to the reference marks from CT and then to assess patient straightening and bladder and rectal contents using a quick low resolution ( $5 \times 5 \times 5 \text{ mm}^3$ ) survey image set. Figure 2.4 demonstrates a typical patient setup on both the CT and MR simulators.

### 2.2.3.1 Contouring Considerations When Using MR as the Secondary Imaging Modality

Secondary MR images for contouring must be of high quality and therefore should be acquired with a field-of-view (FOV) just sufficient to encompass the prostate, seminal vesicles and nearby normal tissues such as the bladder, rectum and penile bulb. A small FOV axial T2w MRI and fiducial identification sequence should be sufficient for this purpose (see Table 2.1). Because the prostate is much smaller on MR compared to CT, CT-MR fusion in the region of the prostate can be quite challenging and the use of stable landmarks that can be observed on both image sets, such as the fiducials, can be particularly helpful for this task (Fig. 2.5 top panel). It should be kept in mind that the seminal vesicles move independently of the prostate and their location may differ on CT and MR depending on rectum and bladder filling

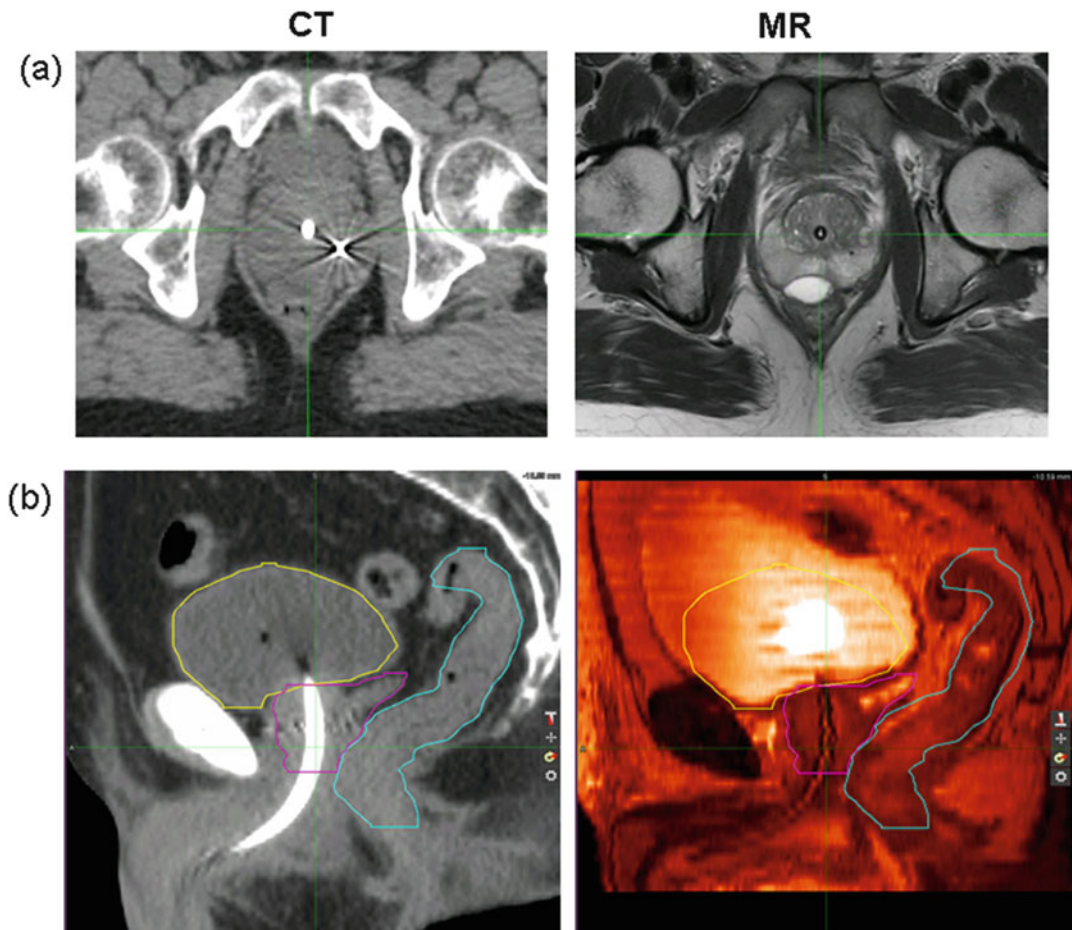
**Table 2.1** MR simulation scanning guideline [64]

Sequences	Coverage	Scan parameters
<i>Sagittal T2</i> 2D TSE (For soft-tissue contouring)	Skin-to-skin (AP) L5 to anal canal (SI) Middle of femoral heads (RL)	
<i>Goldseed</i> Axial 3D BFFE (For fiducial identification)	Covering prostate and seminal vesicles	
<i>MRCAT Source MR</i> Axial 3D FFE mDIXON (For synthetic CT generation)	Skin-to-skin (AP) Skin-to-skin (RL) L4 below to proximal femur (SI)	
<i>Axial T2 small FOV</i> 2D TSE (For soft tissue contouring)	Outer body (AP) Femoral heads (RL) L5 to anal canal (entire rectum) (SI)	
<i>Coronal T2</i> 2D TSE (For soft tissue contouring)	Middle of femoral heads (RL) Entire prostate, bladder neck, rectum (SI) Entire prostate, bladder neck, rectum (AP)	

Abbreviations: *TSE* turbo spin echo, *BFFE* balanced fast field echo, *FFE* fast field echo)

[65, 66]. A larger CTV to PTV margin, especially for high risk patients, may therefore be needed around the seminal vesicles to encompass their position on both CT and MRI and ensure their inclusion within the high dose region. Questions often arise as to which structures should be

segmented on MR when MR is used as the secondary imaging modality. Since, in such a workflow, CT is the primary imaging modality used for planning and image guided delivery, it is advisable to limit MR-based segmentation to the prostate and seminal vesicle target volumes and



**Fig. 2.5** (Top panel) Axial CT+MR fusion based on the implanted gold seed fiducials. Rectal spacer is clearly visible only on the MR. (Bottom panel) Sagittal CT+MR fusion for another patient illustrating contouring

considerations when using MRI as the secondary imaging modality. Note the differences in the size and position of the tissues between the two studies

other secondary structures such as the rectal spacer, penile bulb and urethra (if a Foley catheter is not used) which are clearly visible only on MR. Normal tissues such as the bladder, rectum and bowel should be segmented on CT (Fig. 2.5 bottom panel).

#### 2.2.4 Simulation Workflow 2: MR-Only Simulation

Because of changes in the anatomy (e.g. bladder and rectum filling) that can occur between the acquisition of two image sets and the ambiguity in contouring seminal vesicles, a workflow in

which MRI is the primary and sole imaging modality is preferred over a combined CT and MRI workflow. In addition to minimizing segmentation errors introduced by mis-registration between the CT and MR, an MR-only workflow improves efficiency by reducing the number of imaging sessions, and reduces cost and inconvenience to the patient [43, 64, 67, 68]. However, additional considerations apply to an MR-only workflow including the need to (a) characterize the MR scanner for a larger FOV to ensure images of high geometric fidelity, (b) define a process for MR-only simulation and isocenter marking, (c) commission synthetic CT images generated from single or multiple MR image



sets for high geometric and dosimetric accuracy, (d) define MR acquisition and contouring guidelines and (e) commission a method to obtain 2-D digitally reconstructed radiographs (DRRs) and/or 3-D reference images from MR images with sufficient bone, soft tissue, and/or implanted fiducial visualization to guide image-based patient setup and treatment.

#### 2.2.4.1 MR Scanner Characterization and Routine QA for MR-Only Simulation

MR scanner characterization and imaging protocol requirements for radiation therapy simulation are different and more stringent than those for a diagnostic scanner and therefore, a radiation oncology-specific quality assurance program is needed [44]. Radiation therapy requires images of high geometric fidelity with high spatial and contrast resolution to delineate disease extent and nearby organs at risk. The geometric fidelity of MRI is often questioned due to distortions arising from the scanner (system-specific distortions) or from the patient themselves (patient-specific distortions) [69–71]. Modern MR systems have been designed with tighter system level distortions, primarily those relating to B0 inhomogeneity and gradient nonlinearity due to improved magnet design as well as higher order corrections of gradient non-linearity and high order shimming. For radiation therapy planning, a QA procedure for geometric fidelity operating within a FOV of  $\pm 50$  cm left-right,  $\pm 30$  cm superior–inferior and  $\pm 35$  cm anterior–posterior must be performed routinely to ensure that geometric distortion due to B0 inhomogeneity and gradient linearity do not exceed 2 mm. Patient-specific distortions of  $< 1$  mm have been reported for prostate patients and therefore, this is not a huge concern for MR-based planning [43].

MR simulators are also equipped with an external laser positioning system (ELPS) used to set up the patient to a specific location or to reference marks (skin tattoos) defined during CT simulation. The sagittal and coronal lasers help to evaluate and correct patient rotation. The ELPS are calibrated to send the patient directly to the scanner isocenter, similar to those on a CT

simulator. A daily laser QA procedure should be performed to ensure the laser positions and the distance between the external laser position and the MR bore isocenter are within tolerance. The acceptance criteria should be  $< 2$  mm. A daily ELPS QA and biweekly geometric fidelity QA program is in place at our institution as part of our MR-only workflow.

#### 2.2.4.2 MR-Only Simulation and Isocenter Marking

Although modern MR scanners can be equipped with an external laser positioning system, flat table top and coil bridge supports to perform MR simulation, there are additional requirements for MR-only simulation. These include a water bath in the vicinity of the MR scanner or the use of a slow dry mold for immobilization devices and an MR-compatible method for placing skin tattoos. It is important to note that allowing any immobilization mold to dry completely before imaging is necessary from an MRI safety perspective.

Unlike CT simulators, current MR simulation platforms do not provide virtual simulation capabilities for absolute isocenter marking. For MR-only simulation, a third party software such as MIM MAESTRO<sup>®</sup>,<sup>4</sup> or Eclipse<sup>™</sup>,<sup>5</sup> can be utilized if desired. At our institution, patients have their immobilization device constructed in the CT simulator which provides the additional benefit of allowing us to place initial tattoos at that time, thus providing a relative isocenter to serve as the reference for the MR simulation. A pair of orthogonal CT scout images is also acquired for use during a later QA step during which the locations of the three implanted fiducial markers on the MR images are verified against the CT scout. Three MR-compatible radio opaque Beekley<sup>™</sup><sup>6</sup> markers (BBs) are placed on the initial reference tattoos in MR so that they are visible on the large FOV images. These markers are later used to create an isocenter at the triangulation point.

<sup>4</sup>MIM Software Inc. Cleveland, OH 44122.

<sup>5</sup>Varian Medical Systems, Palo Alto, CA 94304.

<sup>6</sup>Beekley Inc., Bristol, CT 06010.

### 2.2.4.3 Synthetic CT Generation

The lack of electron density information on the MR images is somewhat overcome by the use of synthetic CTs that are generated from these MR images. Various methods have been developed over the last few years to generate synthetic CTs from MR images for prostate radiotherapy. These methods can be broadly classified into:

- (a) Bulk density assignment methods: These methods rely on manual contouring of structures. They provide reasonable accuracy but are not practical for routine use. Dose differences greater than 2.5% to the target have been reported with this method [67, 72, 73].
- (b) Atlas-based methods: These methods rely on the generation of electron density maps from an atlas of co-registered CT and MR images. Large anatomical variation outside that captured in the atlas may compromise the accuracy of atlas based methods due to the limitations of deformable registration [47, 48].
- (c) Classification-based methods: These methods rely on the use of a single or multiple MR sequences to classify the tissue types [43, 45, 46, 74, 75], with the inclusion of a bone atlas to further guide the classification [75, 76]. Such methods are practical for routine use and not limited by variation between patient anatomies. Both atlas-based and classification-based methods have reported a dosimetric accuracy of less than 1% when compared to CT based plans.

In addition to the synthetic CTs developed by different research groups, there are also two commercial options available for clinical use of synthetic CTs. One of them is a classification-based method called MRCAT<sup>7</sup> or MR for Calculating ATtenuation which is limited to a Philips MR scanner [77]. The other method (MRIplanner<sup>8</sup>) is scanner independent and currently only CE

marked for clinical use in Europe [78]. Figure 2.6 shows an example case comparing synthetic CT, source MR and the original CT. Regardless of the synthetic CT method used, the synthetic CT images should be thoroughly commissioned for their geometric and dosimetric accuracy before using them clinically [43, 46, 78, 79]. Ideally, the synthetic CT generation method should be scanner and, if possible, sequence independent so that it could be widely adopted in the clinic. It goes without saying that the DICOM tags of the synthetic CTs must be configured and automatically set to indicate a “CT” imaging modality to allow for a streamlined export of the synthetic CT DICOM images to the treatment planning system (TPS) for dose calculation.

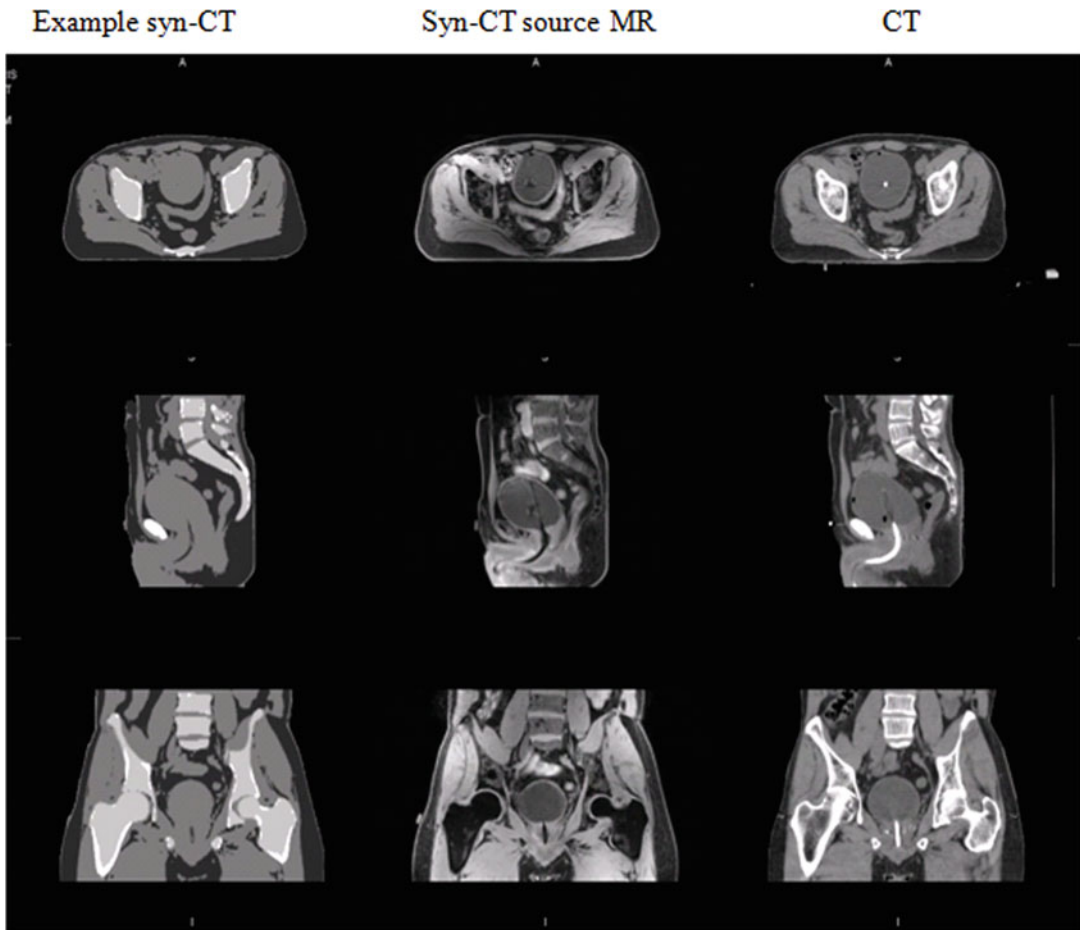
### 2.2.4.4 MR Acquisition and Contouring Guidelines

MR images with sufficient soft tissue contrast are needed for contouring both target and normal structures for MR-only workflow. Ideally, for efficient MR-only simulation, a single MR series could be used to generate the synthetic CTs while also providing sufficient soft tissue contrast to contour the target, normal structures and fiducials. This is currently not possible and most institutions rely on multiple MR series to achieve this. Table 2.1 shows the MR scanning guidelines at MSKCC for MR-only simulation of the prostate using a Philips 3T Ingenia<sup>9</sup> MR scanner. Images are acquired in the following order to minimize the possibility of motion between the adjacent sequences: T2w sagittal, Goldseed visualization, Synthetic CT, T2w axial, T2w coronal. It should be remembered that the ELPS must be turned off prior to scanning as it may otherwise introduce an image artifact [42]. While the MR images are being acquired, an initial image quality assessment is done by the MR technologists to ensure sufficient quality for contouring and gold seed fiducial visualization. The MR technologists are instructed to repeat any acquisition during which significant motion was observed.

<sup>7</sup> Philips Healthcare NA, Cleveland, OH.

<sup>8</sup> Spectronic Medical AB.

<sup>9</sup> Philips Healthcare NA, Cleveland, OH.

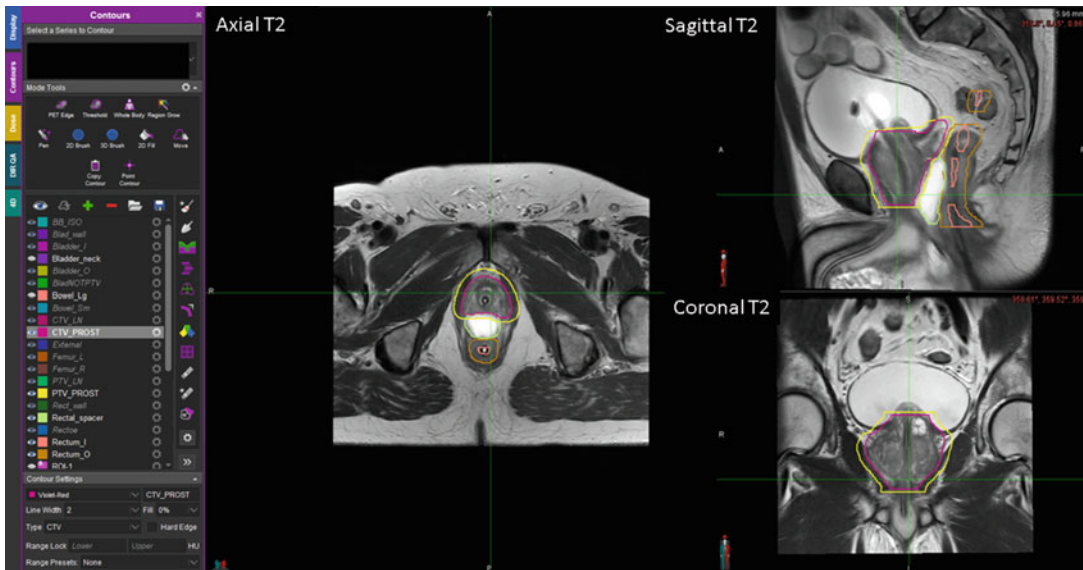


**Fig. 2.6** Example of a synthetic CT, synthetic CT source MR and actual CT of a prostate patient

Motion-induced artifact is currently the biggest technical limitation of MR-only simulation. The development of motion-robust sequences may overcome this challenge in the near future.

Since there are multiple MR datasets for contouring, there is a strong need for an organized workflow to streamline inter-sequence registration and generate automatic image layouts for physicians. The total time for MR simulation is approximately 25 min, during which movement of the prostate and slight changes to bladder and rectal filling can occur. At MSKCC, we have developed a MIM-based contouring workflow that allows us to automatically break the DICOM frame of reference between the MR

series and perform initial inter-sequence registration before contouring. Our MR-only workflows also provide a significant advantage for contouring both target and normal tissue structures from a single imaging modality through the creation of these multi-image page layouts as shown in Fig. 2.7. Physicians contour the CTV (prostate and seminal vesicles), bladder, bladder trigone, bowel, urethra, rectum, and rectal spacer on axial T2 MR images. Fiducials are identified on the Goldseed sequence and femurs on the synthetic CTs. The workflow ensures that all contours are automatically saved on the synthetic CT even though segmentation is done on the MR images exclusively.



**Fig. 2.7** Example physician contouring layout for the MR-only workflow. The layout displays native axial, sagittal and coronal MRI to facilitate contouring. The

contours drawn on these MR images are automatically saved to the synthetic CT

### 2.2.4.5 Planar and Volumetric IGRT Using MR Only

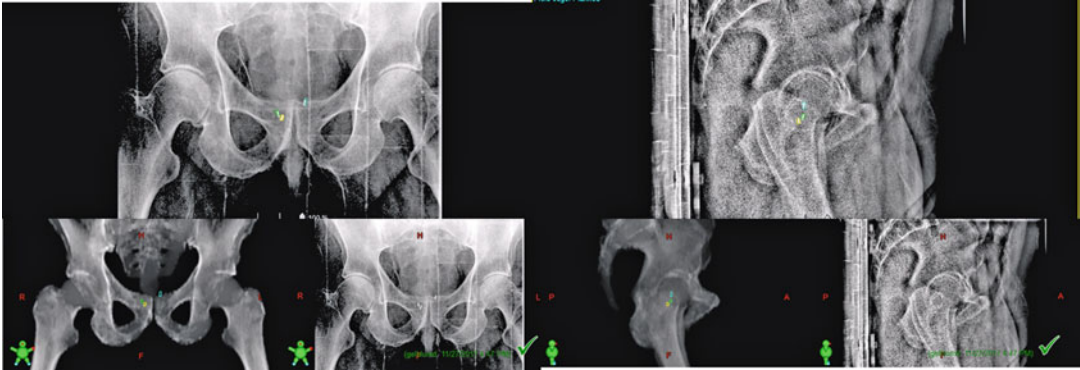
In addition to the dosimetric accuracy, geometric accuracy of synthetic CTs for patient positioning is also very crucial. Planar and volumetric IGRT for prostate patients is performed using 2D DRRs and 3D CBCT. The reference bony DRRs generated from synthetic CTs must be verified with respect to CT based DRRs and commissioned for clinical use [43, 79]. Patient positioning is also often performed based on implanted gold fiducials. An ideal MR sequence should display sharp signal void in the implanted fiducials and show excellent contrast between fiducials and prostate to facilitate an accurate localization of fiducials. Phantom experiments must be performed to verify that the uncertainty in fiducial marker localization due to susceptibility does not exceed the fiducial location identified on the CT ground truth. Table 2.1 shows an example of a 3D balanced fast field echo sequence on a Philips scanner where T1/T2 dependence of the sequence, a sharp signal void and susceptibility of implanted fiducials yields a distinct contrast between the fiducials and nearby

anatomy. Figure 2.8 shows an example of AP and lateral DRRs generated from a synthetic CT and compared with the on-treatment radiographs. The fiducials on the synthetic CT are represented as ROIs and not synthetically generated, although it is also possible to generate the synthetic fiducials on the synthetic CT if one desires. 3D CBCTs are also matched to the reference synthetic CTs based on fiducials. At our institution, the physicians also use the reference planning image to ensure reproducibility of the bladder and rectal filling on the pre-treatment CBCT. If the bladder and rectum contrast is not sufficient on synthetic CTs, physicians can also load the synthetic CT source MR on the on-board imaging console or the Varian ARIA™ offline review module.

## 2.3 General Planning Considerations for SBRT

With the advent of image guided radiotherapy (IGRT), volume modulated arc therapy (VMAT) and most recently, MR-guided or MR-based simulation, treatment planning for hypofractionated





**Fig. 2.8** Example AP and lateral DRRs generated from synthetic CT compared to on-treatment radiographs. The fiducials on the planning DRRs are displayed as ROIs

prostate cancer has evolved toward smaller treatment volumes and margins and tighter dose conformity; attributes that diverge significantly from historical approaches for conventionally fractionated treatment paradigms. This evolution has been facilitated by several technological advances:

1. The incorporation of MRI into the planning process resulting, on average, in a 30–40% decrease in prostate CTV volume.
2. A strong emphasis on patient bowel and bladder preparation applied consistently throughout the course of radiotherapy and the introduction of anatomic modulators (e.g. rectal spacer gels) to successfully implement smaller margins.
3. The widespread adoption of volume modulated arc therapy (VMAT) to increase dose conformity and reduce overall treatment delivery time by up to 50–60%, thereby facilitating margin reduction since shorter times result in less motion.
4. The routine use of daily pre-treatment image guidance using orthogonal radiographs, daily cone beam CT (CBCT) or both, to reduce margins.

Programmatic focus on all of these radiotherapy process aspects (patient preparation, imaging, simulation, planning and treatment delivery) has allowed us to decrease our CTV-to-PTV margins over time from circumferential 10 mm with 6 mm

at the prostate-rectal interface prior to daily pre-treatment IGRT, to circumferential 6 mm with daily IGRT, and most recently to circumferential 5 mm with 3 mm at the prostate-rectal interface for SBRT patients receiving MR simulation, pre-treatment and intra-treatment motion monitoring. If the pelvis will be treated, a 5 mm or larger margin should be considered for the nodal CTVs in recognition of the fact that image-guided setup is focused on the prostate itself and that suboptimal dosimetric coverage of the nodal volumes is possible for patients with large differences in their bony and fiducial registrations and/or bladder filling observed at pre-treatment imaging [80].

For a combined CT and MR workflow, the final plan as well as the DRRs are generated based on the planning CT using the MR-based contours (Sect. 2.2.3.1). In case of an MR-only workflow, plans as well as DRRs are generated using the synthetic CT as the primary image set. An automated workflow ensures that all contours including the fiducial ROIs are automatically saved on the synthetic CT for planning (Sects. 2.2.4.4 and 2.2.4.5).

### 2.3.1 Volume Modulated Arc Therapy Planning for SBRT Prostate Radiotherapy

Volume modulated arc therapy (VMAT), whereby intensity modulated radiotherapy is delivered through a combination of dynamic

motion of the gantry and multileaf collimator and, often, simultaneous modulation of the dose rate has become a widely adopted planning and delivery method for prostate SBRT. Advantages include excellent dose conformity and reduced treatment delivery times which are important to reduce intra-treatment motion. Total in-room time and time from first beam on to last beam off with static field IMRT can exceed 15 and 10 min, respectively. With VMAT, these times can be reduced by approximately 40–50%. Several studies have compared dose distributions of static coplanar field intensity modulation (IMRT) and VMAT [24, 26, 81]. The study of 292 patients by Kopp et al. [81] is representative of the results in that it found that VMAT provided a higher level of conformity leading to decreases in high dose levels to the rectum and bladder. Bladder doses were lower at all volume levels evaluated while the volume of the rectum receiving intermediate doses was the same as IMRT but volumes receiving lower doses were higher. Doses to other evaluated normal tissues including the penile bulb and femoral heads were lower with VMAT, at least at selected volumes and/or dose levels.

VMAT dose distributions have also been compared to other methods used for prostate SBRT, most notably robotic radiosurgery (e.g. CyberKnife<sup>®10</sup>). In a study of eight patients comparing robotic radiosurgery, non-coplanar fixed field IMRT, and two commercially available VMAT methods, Seppala et al. [82], found higher target dose inhomogeneity and mean doses to the bladder and penile bulb with robotic radiotherapy but no significant difference in doses to the other normal tissues between any of the techniques. Dose conformity was best with one of the VMAT implementations and the VMAT techniques, in general, resulted in the lowest number of monitor units (MU). The conclusion of the study was that overall, the dosimetric differences between the techniques were small and therefore, accuracy and time required to deliver the treatment should be the dominant concerns when selecting a technique.

In the following sections, a brief overview of the VMAT planning process for prostate SBRT at MSKCC is provided.

### 2.3.1.1 Preparation for Planning and Generation of Optimization Structures

In addition to segmenting the target and organs-at-risk (OAR) (Sects. 2.2.3.1 and 2.2.4.4), optimization control structures such as rinds or shells can be created and used to control the dose distribution, particularly the dose fall-off beyond the target, during optimization. Optimization control structures created from logical combinations or expansions of other structures (e.g. PTV-rectum overlap, Urethra plus 2 mm) are also extremely helpful for controlling dose fall-off, hot or cold spots in specific parts of the plan. When using nested structures for optimization, as is common with control shells or targets with different dose levels for simultaneous integrated boost plans, results are often better if a small gap is left between adjacent structures. Other optimization control structures may be necessary for cases requiring pelvic nodal irradiation, a cone down or boost to a portion of the prostate CTV, or for cases where external beam radiotherapy is being delivered after a brachytherapy implant. Table 2.2 provides a few examples of optimization control structures which can be helpful for prostate SBRT planning scenarios.

### 2.3.1.2 SBRT VMAT Planning for Intact Prostate Patients

Typically, two full 360° arcs are used for prostate SBRT which are directed from the clockwise and counterclockwise directions and use collimator angles offset by approximately 90° to provide additional degrees of freedom during optimization and to minimize tongue and groove effects. In the presence of hip prostheses, skip arcs which prevent direct beam entry through the prosthetic device can be considered. However, in such a scenario, IMRT with seven to nine fixed fields may still be particularly useful due to the ability to more carefully control the beam directions and dose entering through the prosthetic devices. By using asymmetric jaws, isocenter placement in

<sup>10</sup> Accuray, Sunnyvale, CA.

**Table 2.2** Examples of optimization control structures for SBRT radiotherapy of the intact prostate

Structure name	Structure definition	Structure purpose
PTV_Opt	Prostate PTV excluding OARs (PTV_Prostate <i>not</i> Rectum <i>not</i> Urethra <i>not</i> Bladder Trigone)	Control of PTV coverage
PTV_Bladder	Intersection of Prostate PTV and Bladder (PTV_Prostate <i>and</i> Bladder)	Control of PTV coverage and dose gradient between the PTV and bladder
Rind1	Axial expansion of PTV (PTV + 3 cm) <i>not</i> (PTV + 0.3 cm)	Control of dose falloff
Rind2	Axial expansion of Rind1 (RIND1 + 3 cm) <i>not</i> (RIND1 + 0.1 cm)	Control of dose falloff
Urethra_Ext	Axial and longitudinal expansion of Urethra (Urethra + 0.2 cm), Extend longitudinally beyond PTV by ~0.5 cm	Control of urethral dose

the center of the prostate works well for the vast majority of prostate SBRT cases, including those requiring nodal irradiation. Most commercial treatment planning systems allow for the creation of field definition templates which define basic field parameters including arc length, gantry start and stop angles, and collimator angles. Scripting may provide for more automation at this step in the planning process such that with little effort, the initial treatment fields can be prepared.

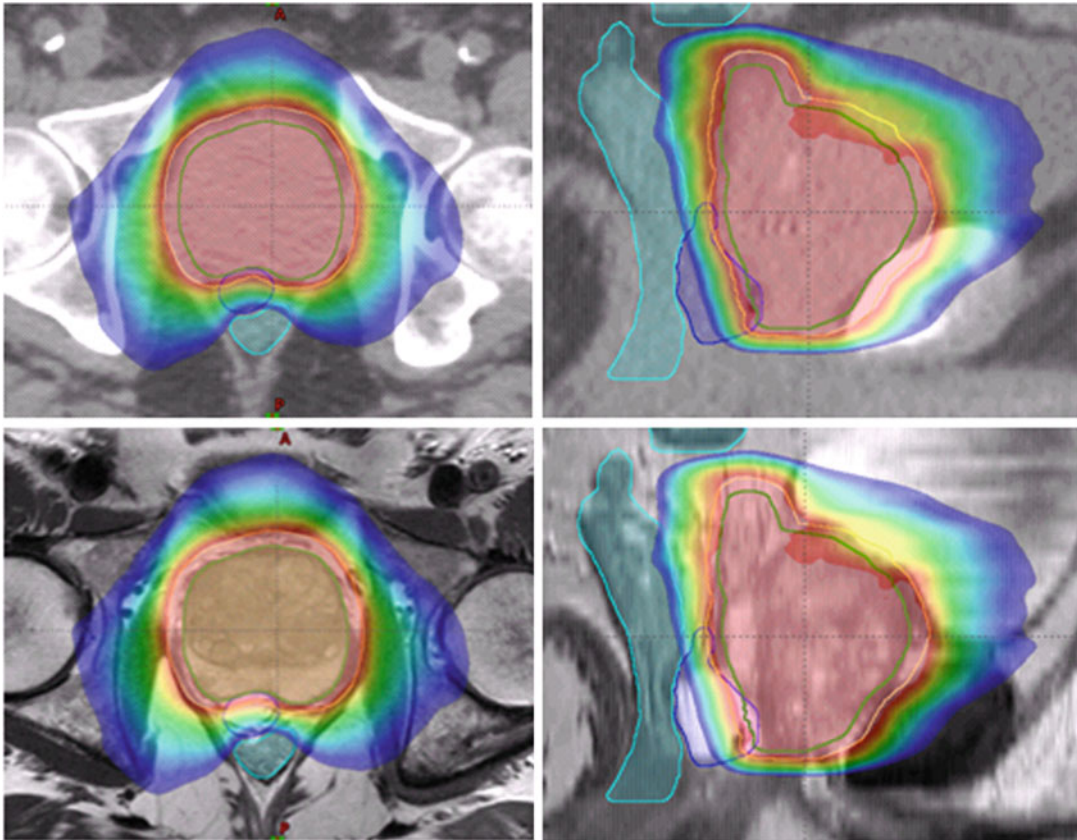
In virtually all treatment planning systems, VMAT optimization is initiated from a template of dose and volume objectives and priorities for the targets and normal tissues. Typically, maximum, minimum and dose volume objectives are used for the target and OARs (rectum, bladder, penile bulb, femoral heads) which are quite similar to but not necessarily identical to the clinical criteria that will be used to evaluate the quality of the plan. Optimization control structures including rinds, shells or Boolean structures are typically applied with relatively light priority. Analytical methods for controlling dose fall-off outside of the target such as the normal tissue objective (NTO) are also often very helpful during optimization [83].

Figures 2.9 and 2.10 illustrate typical VMAT dose distributions for prostate patients with and without rectal spacers receiving 40 Gy in five fractions. A comparison of the dose volume histograms (DVHs) is given in Fig. 2.11. For both patients, MRI was used to define the prostatic target yielding CTV volumes of 128 and 94 cc. Excellent, highly conformal coverage of

the target and sparing of the rectum is possible in the presence of the rectal spacer which is clearly visible only on the MRI (Fig. 2.9). The loss of coverage at the prostate-bladder interface in this patient was a consequence of a dosimetric constraint placed on the dose to the bladder and bladder trigone. Coverage of the target is excellent as well for the patient without rectal spacer (Fig. 2.10) but at the cost of a higher dose to the rectum. Dose volume histograms of the PTV, rectum and bladder for both patients are compared in Fig. 2.11 demonstrating the advantage in rectal dose obtained with the spacer.

The current MSK criteria for evaluation of SBRT plans delivering 40 Gy in five fractions are provided in Table 2.3. For patients receiving slightly different fractionations, the absolute doses to the normal tissues are scaled up or down when clinically appropriate and physically possible. For example, for a fractionation of 37.5 Gy in five fractions, the PTV maximum dose and D95% criteria and the dose criteria for the rectum, bladder, skin, penile bulb and urethra are all proportionally lower than the 40 Gy criteria. However, the bowel doses are the same since at the time that we escalated the SBRT prescription from 37.5 to 40 Gy, clinical prudence dictated that the bowel criteria remain unchanged.

Similar criteria for evaluating plan quality have been developed by other institutions and cooperative groups. It should be remembered that dose volume metrics, structure segmentation and planning guidelines are interrelated and have often been developed from clinical practice over



**Fig. 2.9** Axial and sagittal VMAT dose distributions for a patient with a rectal spacer undergoing 40 Gy SBRT radiotherapy. The plan is shown on CT (top) and MR T2 (bottom) images. Structures indicated include the PTV

(yellow), CTV (green), rectal spacer (purple) and rectum (cyan). The colorwash isodoses range from 20 Gy (blue) to 40 Gy (red)

many years. As a result, the adoption of specific dose volume metrics such as those listed in Table 2.3 should only be done in the context of developing a larger program that evaluates all aspects of the planning process.

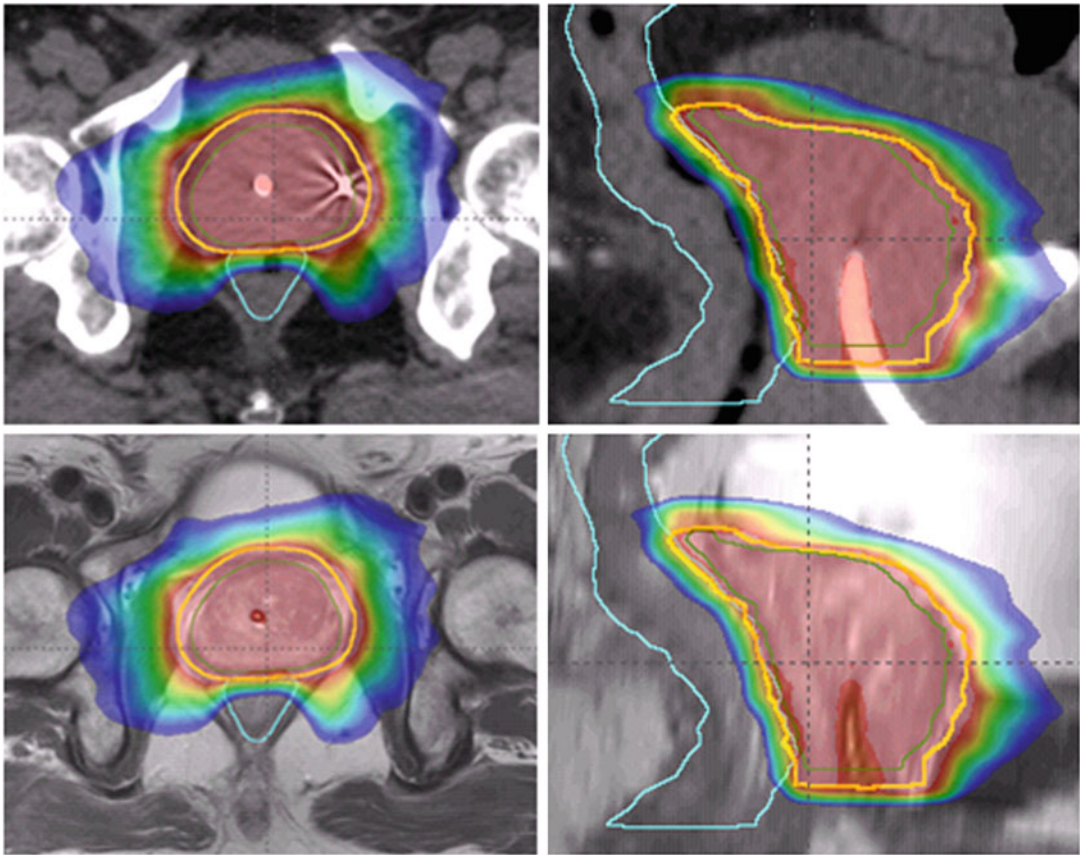
SBRT is also being used, although not yet as widely, for other scenarios including in combination with LDR or HDR brachytherapy, when treating the pelvic lymph nodes, and for salvage treatment after prostatectomy or initial radiotherapy. Although the doses, plan evaluation metrics and criteria are quite different from the prostate-only approach described above, other aspects of the planning approach are very similar, particularly with regard to the segmentation of targets, normal tissues, beam arrangement and optimization structures.

## 2.4 Future Developments in Prostate SBRT Simulation and Planning

### 2.4.1 Segmentation and Focal Dose Escalation of the Dominant Intra-Prostatic Lesion (DIL)

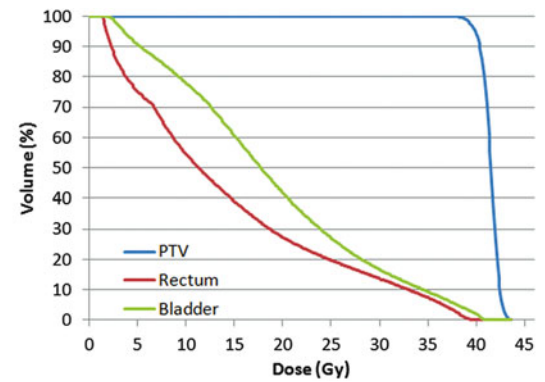
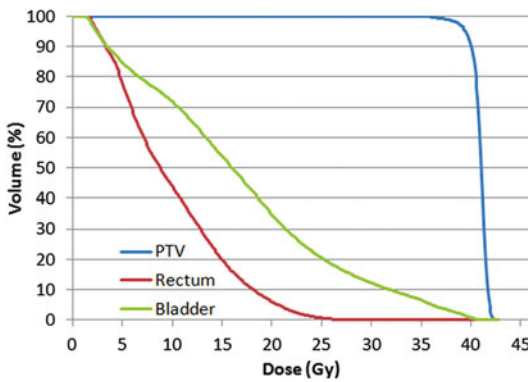
There continues to be intense interest in identifying men who would benefit from segmental or focal therapies targeting dominant or index lesions within the prostate in an effort to avoid overtreatment and limit urinary and sexual function toxicity. It is clear that local failures after external beam radiotherapy tend to occur at the site of the original index lesion providing





**Fig. 2.10** Axial and sagittal VMAT dose distributions for a patient without a rectal spacer undergoing 40 Gy SBRT radiotherapy. The plan is shown on CT (top) and MR T2

(bottom) images. Structures indicated include the PTV (yellow), CTV (green), and rectum (cyan). The colorwash isodoses range from 20 Gy (blue) to 40 Gy (red)



**Fig. 2.11** Typical Dose Volume Histograms (DVHs) for the prostate planning target volume (PTV), rectum and bladder for patients with and without rectal spacers undergoing 40 Gy SBRT radiotherapy

**Table 2.3** MSKCC plan evaluation criteria for SBRT extreme hypofractionation regimen of 40 Gy in five fractions

Structure	Metric	Criteria
PTV	Mean dose	101–103% (Acceptable range)
	Maximum dose	42.8 Gy (Acceptable) 44 Gy (Limit)
	D <sub>95%</sub>	40 Gy (Ideal) 36.25 Gy (Limit)
	Minimum dose	33.7 Gy–34.4 Gy
Rectum	Max dose	≤41.2 Gy
	D <sub>1 cc</sub>	≤38.5 Gy
	Mean dose	13 Gy (Ideal) 16.4 Gy (Limit)
	V <sub>24 Gy</sub>	≤25%
	V <sub>30.15 Gy</sub>	≤8 cc
	V <sub>10 Gy</sub>	≤52% (Guideline only)
Bladder	Max dose	42 Gy
	D <sub>10%</sub>	36 Gy
	D <sub>50%</sub>	20 Gy
Bladder trigone	Max dose	38 Gy
Urethra	Max dose	42 Gy
	D <sub>1 cc</sub>	40 Gy
Femoral heads	Max dose	31 Gy
	D <sub>10 cc</sub>	21.6 Gy
Skin	Max dose	32.4 Gy
Penile bulb	Max dose	40 Gy
	D <sub>3 cc</sub>	21.6 Gy
Large bowel	Max dose	29 Gy
Small bowel	Max dose	25 Gy

justification for further dose escalation to that area [84, 85]. Several groups have evaluated the use of multi-parametric MRI imaging and intensity modulated external beam monotherapy to identify and boost the radiation dose to the dominant lesion [12–15, 86]. Four of these studies boosted the dominant lesion under a conventional fractionation paradigm with doses ranging from 80 Gy in 40 fractions to 95 Gy in 35 fractions. Aluwini et al. [86] used the CyberKnife technology to perform an extreme hypofractionated regimen of 38 Gy in four fractions to the entire prostate and a boost of up to 11 Gy (total dose = 49 Gy) to the MRI-identified dominant tumor. The study was comprised of 50 patients with dominant lesions identified in 14. Although the dosimetric constraints imposed in the study were achieved for most patients, 30% had minor deviations, highlighting the technical challenges in this aggressive approach. All investigators concluded however that boosting the dominant

lesion was technically feasible and resulted in toxicity profiles similar to those of whole-prostate conventional fractionation approaches.

Multi-parametric MR imaging has been the predominant imaging method evaluated for the purposes of differentiating tumor from surrounding normal prostatic tissue and segmenting the dominant lesions targeted for focal therapy. Specifically, T2-weighted imaging for localization based on anatomic visualization and diffusion-weighted (DWI), perfusion (DCE) and spectroscopic MRI for localization based on functional characteristics have all been fairly extensively studied. Although spectroscopy exhibits good specificity, the spatial resolution remains inadequate for planning purposes and it is used infrequently. On the other hand, specificity and sensitivity can be improved by including the complementary information from a combination of T2, diffusion and perfusion imaging. Groenendaal et al. [87] have studied the

congruence between tumor segmentations with diffusion and perfusion imaging using receiver operating curve (ROC) analyses and applying one or the other of the imaging sequences with multiple threshold values as the reference. Although excellent area under the curve (AUC) values were obtained for select patients, the average AUC value was only 0.6 with single imaging datasets, demonstrating a relatively low overlap between the two imaging methods and the possible advantage of using combined data.

Validation of MR-based localization through comparison with gold-standard pathology is technically challenging. Groenendaal et al. [88] segmented tumor tissue on T2, diffusion and perfusion imaging for five patients prior to prostatectomy and subsequently registered those delineations to tumor tissue delineated on the whole mount hematoxylin-eosin stained (H&E) sections. Congruence between the two methods was only 45–89% but addition of a 5 mm margin on the MR-based segmentations increased this to 85–100%. Only 2–3 mm of the MR margin was felt to be related to the MR-to-pathology registration uncertainty.

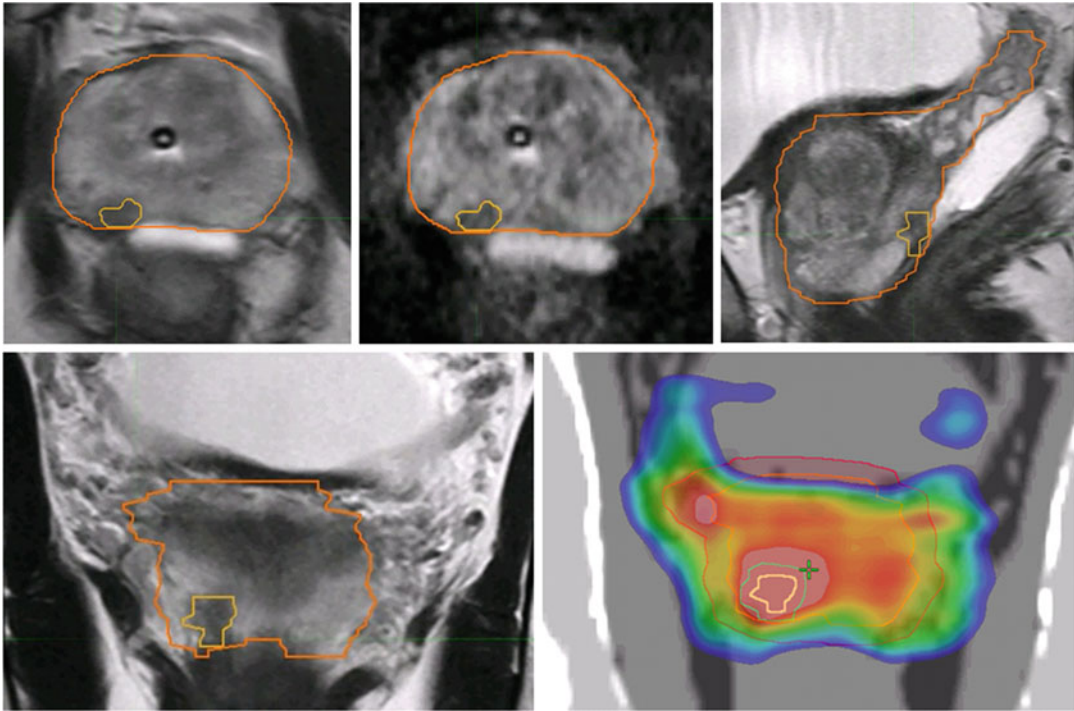
Several groups have pointed out the need to better understand the relationship between the parameters extracted from diffusion and perfusion imaging and the underlying structure and physiology of the prostate tissue. Doing so should strengthen our interpretation of the information provided by each and allow us to establish appropriate thresholds or other methods for classifying individual voxels as tumorous. Several studies have looked at the overall relationship between apparent diffusion coefficient and cell density within the prostate [89–92] with the results showing moderately strong correlations. Researchers from the University Medical Center Utrecht [93] investigated the voxel-level relationship between the apparent diffusion coefficient (ADC) and tissue features including cell density and presence of glandular tissue. They concluded that, at the voxel level, there exists significant heterogeneity of cell density and glandular tissue within normal prostate tissue and tumors that is reflected in the heterogeneity of the ADC map. Furthermore, for small tumors specifically, ADC

values did not adequately reflect the histopathological features, perhaps due to partial volume effects, leading the authors to conclude that small tumors or parts of tumors might be missed on an ADC map.

In further recognition of the fact that T2, diffusion and perfusion imaging may be providing complementary information valuable for segmentation of the prostatic tumor, some groups are attempting to build quantitative models based on a voxel-level determination of tumor-bearing probability and to use those models to inform dominant lesion segmentation [36, 94–98]. For example, Groenendaal et al. [96] developed a logistic regression model using local statistics obtained from parameters from diffusion and perfusion imaging on 87 radiotherapy patients to predict tumor presence on a voxel level. After validation using prostatectomy patients, a method was also developed to stratify voxels into gross tumor volume (GTV), high risk clinical target volume (CTV) and low risk CTV based on tumor probability. Viswanath et al. [97] used texture features extracted from T2-weighted images. Dinh et al. [98] used over 30 features from multi-parametric MR, each patient's biopsy map and a population-based tumor probability atlas to create a model that was validated on a voxel level against pathology. Their results demonstrated an AUC of 0.78 when all features were combined and evaluated on patients from two institutions.

Although, as described above, the use of multi-parametric MRI alone or in combination with other features to automatically guide tumor segmentation for focal prostate radiotherapy is promising, it must still be considered investigational. Therefore, most ongoing clinical studies evaluating the role of focal irradiation of index lesions, are utilizing multi-parametric MR imaging with expert radiologist evaluation to define the tumor region [13, 14, 16].

At MSKCC, a Phase I study evaluating the feasibility of radiotherapy to the prostate and dominant intra-prostatic lesion using extreme hypofractionated, MR-guided SBRT is underway. The specific aims of this study are to assess the feasibility and toxicity of such treatment for



**Fig. 2.12** (Top panel) Axial and sagittal T2-weighted images and axial DWI ADC map for a patient undergoing extreme hypofractionated SBRT with a simultaneous boost to the intra-prostatic dominant lesion (DIL). (Lower panel) Coronal T2-weighted image and corresponding synthetic CT image with overlaid VMAT dose distribution designed to deliver 40 Gy in five

fractions to the prostate and 45 Gy in five fractions to the DIL. The colorwash isodoses range from 30 Gy (blue) to 45 Gy (red). For all panels, the DIL and prostate and seminal vesicles are shown in yellow and orange, respectively. The PTVs for the DIL and prostate are shown in green and red

intermediate risk patients with a regimen that consists of 45 Gy in five fractions to the dominant lesion and 40 Gy to as much of the remaining prostate as possible given strict normal tissue constraints to the bladder, bladder trigone, penile bulb and neurovascular bundles. Several weeks prior to the simulation, the patient undergoes a single procedure during which gold seed fiducials and a rectal spacer are implanted to aid with later image-guided treatment delivery and reduction of the rectal dose. Patients then undergo multiparametric MR imaging and MR-only simulation as described in the previous sections. A radiologist and radiation oncologist jointly review the MR images to define the dominant lesion PTV and a VMAT plan is then developed using methods similar to those described in Sect. 2.3. At the time of treatment, patients are set up using on-board, fiducial-guided kilovoltage imaging.

Correct positioning, bladder and rectal filling are confirmed with cone beam CT (CBCT) registered to the synthetic CT and/or source MR images. Simultaneous megavoltage and kilovoltage imaging during treatment is used to track the prostate position from the gold seed fiducials with treatment interruption if positional shifts of  $>1.5$  mm/10 s are observed [55]. An example of MR images and the VMAT plan incorporating DIL irradiation for one patient is shown in Fig. 2.12.

#### 2.4.2 Adaptive Planning and MR-Guided Treatment Delivery

As discussed earlier, the combined use of MR-only treatment planning and image guidance for patient setup and monitoring of motion during treatment has allowed us to decrease the margin



around the prostate target and facilitated extreme hypofractionated treatment approaches. Further technological progress in the near future will support on-line adaptive re-planning and MR-guided delivery. Dose delivery at each session will be able to conform to the prostate and normal tissue “position-of-the-day” and treatment delivery gated using real-time MR-guidance will ensure that the high dose region adheres to an increasingly tight margin around the target.

Several groups have investigated the feasibility of on-line adaptive prostate radiotherapy using approaches such as plan libraries [99, 100] and MLC segment shape and weight modification [101–105]. Plan library approaches generate a series of plans a priori to reflect the most likely anatomical configurations between the prostate and other relevant tissues including the pelvic lymph nodes, rectum and bladder. At each treatment session, the most appropriate plan is then selected for delivery based on a measure of similarity between the simulation and treatment image sets such as mutual information. Qi et al. [99] evaluated the dosimetric advantages that could be expected by being able to select at each treatment session from any of nine available plans designed to accommodate typical changes in the superior–inferior and anterior–posterior position of the prostate with respect to the pelvic lymph nodes. Compared to the typical approach which merely shifts the isocenter based on the daily image-guided setup, a library-based adaptive approach maintained coverage of the prostate but improved coverage of the pelvis. Although the dosimetric results with full online re-optimization were still better, an a priori plan library approach can potentially be implemented with fewer resources and/or changes to the record and verify system or linac treatment console. MLC segment modification approaches have been proposed that rely on deformable registration between the images acquired at simulation and treatment [101] or more simply, a comparison of the target structure outlines [105] to determine the information necessary to morph the MLC segments to better conform to the treatment day geometry. Such approaches can, in theory, more accurately account for rigid body translations and

rotations and deformations than a plan library approach albeit with additional effort at the treatment machine.

Although approaches for adaptive radiotherapy have been proposed, clinical implementation has been lacking due to the challenges of providing robust and efficient software functionality on standard linear accelerators and the relatively poor image quality of cone beam CT (CBCT). With the advent of MR-guided radiotherapy delivery systems (MRgRT) however, these challenges are being addressed and on-line adaptive radiotherapy is becoming increasingly feasible [106]. The superior pre-treatment imaging afforded by MRgRT systems should ultimately facilitate daily plan adaptation not only to the position of the prostate but to the dominant lesion as well. MRgRT systems will also support gated delivery based on real-time imaging, thereby further mitigating dose delivery inaccuracies resulting from intra-treatment motion. In the first version of such a system, the ViewRay MRIdian<sup>11</sup> system is able to monitor motion in a sagittal plane at approximately 4 Hz, perform the necessary deformable image registration, segment the structure and gate delivery based on user defined thresholds combining distance and time criteria. Further development of such systems and their integration with MR-only simulation and planning workflows will most certainly be a major factor in the further adoption and advancement of adaptive hypofractionated SBRT techniques.

---

## References

1. Kupelian PA, et al. Short-course intensity-modulated radiotherapy (70 GY at 2.5 GY per fraction) for localized prostate cancer: preliminary results on late toxicity and quality of life. *Int J Radiat Oncol Biol Phys.* 2001;51(4):988–93.
2. Yeoh EE, et al. Evidence for efficacy without increased toxicity of hypofractionated radiotherapy for prostate carcinoma: early results of a Phase III randomized trial. *Int J Radiat Oncol Biol Phys.* 2003;55(4):943–55.

---

<sup>11</sup> ViewRay, Oakwood Village, Ohio.

3. Pollack A, et al. Dosimetry and preliminary acute toxicity in the first 100 men treated for prostate cancer on a randomized hypofractionation dose escalation trial. *Int J Radiat Oncol Biol Phys.* 2006;64(2):518–26.
4. Kupelian PA, et al. Hypofractionated intensity-modulated radiotherapy (70 Gy at 2.5 Gy per fraction) for localized prostate cancer: Cleveland Clinic experience. *Int J Radiat Oncol Biol Phys.* 2007;68(5):1424–30.
5. Catton CN, et al. Randomized trial of a hypofractionated radiation regimen for the treatment of localized prostate cancer. *J Clin Oncol.* 2017;35(17):1884–90.
6. Arcangeli G, et al. Moderate hypofractionation in high-risk, organ-confined prostate cancer: final results of a phase III randomized trial. *J Clin Oncol.* 2017;35(17):1891–7.
7. King CR, et al. Stereotactic body radiotherapy for localized prostate cancer: interim results of a prospective phase II clinical trial. *Int J Radiat Oncol Biol Phys.* 2009;73(4):1043–8.
8. Alongi F, et al. Linac based SBRT for prostate cancer in 5 fractions with VMAT and flattening filter free beams: preliminary report of a phase II study. *Radiat Oncol.* 2013;8:171.
9. Qi XS, et al. Plan quality and dosimetric association of patient-reported rectal and urinary toxicities for prostate stereotactic body radiotherapy. *Radiother Oncol.* 2016;121(1):113–7.
10. Koskela K, et al. Hypofractionated stereotactic body radiotherapy for localized prostate cancer – first Nordic clinical experience. *Acta Oncol.* 2017;56(7):978–83.
11. Pasquier D, et al. Hypofractionated stereotactic boost in intermediate risk prostate carcinoma: preliminary results of a multicenter phase II trial (CKNO-PRO). *PLoS One.* 2017;12(11):e0187794.
12. Fonteyne V, et al. Intensity-modulated radiotherapy as primary therapy for prostate cancer: report on acute toxicity after dose escalation with simultaneous integrated boost to intraprostatic lesion. *Int J Radiat Oncol Biol Phys.* 2008;72(3):799–807.
13. Lips IM, et al. Single blind randomized phase III trial to investigate the benefit of a focal lesion ablative microboost in prostate cancer (FLAME-trial): study protocol for a randomized controlled trial. *Trials.* 2011;12:255.
14. Ippolito E, et al. Intensity-modulated radiotherapy with simultaneous integrated boost to dominant intraprostatic lesion: preliminary report on toxicity. *Am J Clin Oncol.* 2012;35(2):158–62.
15. Schild MH, et al. Early outcome of prostate intensity modulated radiation therapy (IMRT) incorporating a simultaneous intra-prostatic MRI directed boost. *OMICS J Radiol.* 2014;3:4.
16. Timon G, et al. Rationale and protocol of AIRC IG-13218, short-term radiotherapy for early prostate cancer with concomitant boost to the dominant lesion. *Tumori.* 2016;102(5):536–40.
17. Brenner DJ, Hall EJ. Fractionation and protraction for radiotherapy of prostate carcinoma. *Int J Radiat Oncol Biol Phys.* 1999;43(5):1095–101.
18. Duchesne GM, Peters LJ. What is the alpha/beta ratio for prostate cancer? Rationale for hypofractionated high-dose-rate brachytherapy. *Int J Radiat Oncol Biol Phys.* 1999;44(4):747–8.
19. Dasu A. Is the alpha/beta value for prostate tumours low enough to be safely used in clinical trials? *Clin Oncol (R Coll Radiol).* 2007;19(5):289–301.
20. Nahum AE. The radiobiology of hypofractionation. *Clin Oncol (R Coll Radiol).* 2015;27(5):260–9.
21. Jaffray DA. Image-guided radiotherapy: from current concept to future perspectives. *Nat Rev Clin Oncol.* 2012;9(12):688–99.
22. De Los Santos J, et al. Image guided radiation therapy (IGRT) technologies for radiation therapy localization and delivery. *Int J Radiat Oncol Biol Phys.* 2013;87(1):33–45.
23. Otto K. Volumetric modulated arc therapy: IMRT in a single gantry arc. *Med Phys.* 2008;35(1):310–7.
24. Palma D, et al. Volumetric modulated arc therapy for delivery of prostate radiotherapy: comparison with intensity-modulated radiotherapy and three-dimensional conformal radiotherapy. *Int J Radiat Oncol Biol Phys.* 2008;72(4):996–1001.
25. Shaffer R, et al. Volumetric modulated arc therapy and conventional intensity-modulated radiotherapy for simultaneous maximal intraprostatic boost: a planning comparison study. *Clin Oncol (R Coll Radiol).* 2009;21:401–7.
26. Zhang P, et al. Volumetric modulated arc therapy: planning and evaluation for prostate cancer cases. *Int J Radiat Oncol Biol Phys.* 2010;76(5):1456–62.
27. Khoo VS, Joon DL. New developments in MRI for target volume delineation in radiotherapy. *Br J Radiol.* 2006;79(1):S2–S15.
28. Metcalfe P, et al. The potential for an enhanced role for MRI in radiation-therapy treatment planning. *Technol Cancer Res Treat.* 2013;12(5):429–46.
29. Kupelian P, Sonke JJ. Magnetic resonance-guided adaptive radiotherapy: a solution to the future. *Semin Radiat Oncol.* 2014;24(3):227–32.
30. McGee KP, et al. MRI in radiation oncology: underserved needs. *Magn Reson Med.* 2016;75(1):11–4.
31. Pinkawa M, et al. Application of a spacer gel to optimize three-dimensional conformal and intensity modulated radiotherapy for prostate cancer. *Radiother Oncol.* 2011;100(3):436–41.
32. Pinkawa M, et al. Spacer stability and prostate position variability during radiotherapy for prostate cancer applying a hydrogel to protect the rectal wall. *Radiother Oncol.* 2013;106(2):220–4.
33. Song DY, et al. A multi-institutional clinical trial of rectal dose reduction via injected polyethylene-glycol hydrogel during intensity modulated radiation therapy for prostate cancer: analysis of dosimetric outcomes. *Int J Radiat Oncol Biol Phys.* 2013;87(1):81–7.

34. Uhl M, et al. Absorbable hydrogel spacer use in men undergoing prostate cancer radiotherapy: 12 month toxicity and proctoscopy results of a prospective multicenter phase II trial. *Radiat Oncol.* 2014;9:96.
35. McLaughlin PW, et al. Radiographic and anatomic basis for prostate contouring errors and methods to improve prostate contouring accuracy. *Int J Radiat Oncol Biol Phys.* 2010;76(2):369–78.
36. Ozer S, et al. Supervised and unsupervised methods for prostate cancer segmentation with multispectral MRI. *Med Phys.* 2010;37(4):1873–83.
37. Steenbergen P, et al. Prostate tumor delineation using multiparametric magnetic resonance imaging: inter-observer variability and pathology validation. *Radiother Oncol.* 2015;115(2):186–90.
38. Gao Z, et al. A study of prostate delineation referenced against a gold standard created from the visible human data. *Radiother Oncol.* 2007;85(2):239–46.
39. Rasch C, et al. Definition of the prostate in CT and MRI: a multi-observer study. *Int J Radiat Oncol Biol Phys.* 1999;43(1):57–66.
40. Roach M 3rd, et al. Prostate volumes defined by magnetic resonance imaging and computerized tomographic scans for three-dimensional conformal radiotherapy. *Int J Radiat Oncol Biol Phys.* 1996;35(5):1011–8.
41. Paulson ES, et al. Consensus opinion on MRI simulation for external beam radiation treatment planning. *Radiother Oncol.* 2016;121(2):187–92.
42. Glide-Hurst CK, et al. Initial clinical experience with a radiation oncology dedicated open 1.0T MR-simulation. *J Appl Clin Med Phys.* 2015;16(2):5201.
43. Tyagi N, et al. Dosimetric and workflow evaluation of first commercial synthetic CT software for clinical use in pelvis. *Phys Med Biol.* 2017;62(8):2961–75.
44. Paulson ES, et al. Comprehensive MRI simulation methodology using a dedicated MRI scanner in radiation oncology for external beam radiation treatment planning. *Med Phys.* 2015;42(1):28.
45. Hsu SH, et al. Investigation of a method for generating synthetic CT models from MRI scans of the head and neck for radiation therapy. *Phys Med Biol.* 2013;58(23):8419–35.
46. Korhonen J, et al. A dual model HU conversion from MRI intensity values within and outside of bone segment for MRI-based radiotherapy treatment planning of prostate cancer. *Med Phys.* 2014;41(1):011704.
47. Dowling JA, et al. An atlas-based electron density mapping method for magnetic resonance imaging (MRI)-alone treatment planning and adaptive MRI-based prostate radiation therapy. *Int J Radiat Oncol Biol Phys.* 2012;83(1):e5–11.
48. Chen S, et al. MR image-based synthetic CT for IMRT prostate treatment planning and CBCT image-guided localization. *J Appl Clin Med Phys.* 2016;17(3):236–45.
49. Clemente S, et al. Role of the technical aspects of hypofractionated radiation therapy treatment of prostate cancer: a review. *Int J Radiat Oncol Biol Phys.* 2015;91(1):182–95.
50. Kupelian P, et al. Multi-institutional clinical experience with the Calypso System in localization and continuous, real-time monitoring of the prostate gland during external radiotherapy. *Int J Radiat Oncol Biol Phys.* 2007;67(4):1088–98.
51. Langen KM, et al. Observations on real-time prostate gland motion using electromagnetic tracking. *Int J Radiat Oncol Biol Phys.* 2008;71(4):1084–90.
52. Quigley MM, Mate TP, Sylvester JE. Prostate tumor alignment and continuous, real-time adaptive radiation therapy using electromagnetic fiducials: clinical and cost-utility analyses. *Urol Oncol.* 2009;27(5):473–82.
53. Langen KM, et al. Initial experience with megavoltage (MV) CT guidance for daily prostate alignments. *Int J Radiat Oncol Biol Phys.* 2005;62(5):1517–24.
54. Crook JM, et al. Prostate motion during standard radiotherapy as assessed by fiducial markers. *Radiother Oncol.* 1995;37(1):35–42.
55. Hunt M, et al. Simultaneous MV-kV imaging for intrafractional motion management during volumetric-modulated arc therapy delivery. *J Appl Clin Med Phys.* 2016;17(2):473–86.
56. Hatiboglu G, et al. Application technique: placement of a prostate-rectum spacer in men undergoing prostate radiation therapy. *BJU Int.* 2012;110(11 Pt B):E647–52.
57. Pinkawa M, et al. Quality of life after intensity-modulated radiotherapy for prostate cancer with a hydrogel spacer. Matched-pair analysis. *Strahlenther Onkol.* 2012;188(10):917–25.
58. Weber DC, et al. Intensity modulated proton and photon therapy for early prostate cancer with or without transperineal injection of a polyethylen glycol spacer: a treatment planning comparison study. *Int J Radiat Oncol Biol Phys.* 2012;84(3):e311–8.
59. Ten Haken RK, et al. Treatment planning issues related to prostate movement in response to differential filling of the rectum and bladder. *Int J Radiat Oncol Biol Phys.* 1991;20(6):1317–24.
60. Algan O, et al. The dosimetric impact of daily setup error on target volumes and surrounding normal tissue in the treatment of prostate cancer with intensity-modulated radiation therapy. *Med Dosim.* 2012;37(4):406–11.
61. Steenbakkens RJ, et al. Impact of knee support and shape of tabletop on rectum and prostate position. *Int J Radiat Oncol Biol Phys.* 2004;60(5):1364–72.
62. Sun J, et al. Investigation on the performance of dedicated radiotherapy positioning devices for MR scanning for prostate planning. *J Appl Clin Med Phys.* 2015;16(2):4848.
63. Hanvey S, et al. The influence of MRI scan position on image registration accuracy, target delineation and

- calculated dose in prostatic radiotherapy. *Br J Radiol.* 2012;85(1020):e1256–62.
64. Tyagi N, et al. Clinical workflow for MR-only simulation and planning in prostate. *Radiat Oncol.* 2017;12(1):119.
  65. Mak D, et al. Seminal vesicle interfraction displacement and margins in image guided radiotherapy for prostate cancer. *Radiat Oncol.* 2012;7:139.
  66. Gill S, et al. Seminal vesicle intrafraction motion analysed with cinematic magnetic resonance imaging. *Radiat Oncol.* 2014;9:174.
  67. Lambert J, et al. MRI-guided prostate radiation therapy planning: Investigation of dosimetric accuracy of MRI-based dose planning. *Radiother Oncol.* 2011;98(3):330–4.
  68. Korhonen J, et al. Clinical experiences of treating prostate cancer patients with magnetic resonance imaging-only based radiation therapy treatment planning workflow. *Int J Radiat Oncol Biol Phys.* 2016;96(2):S225.
  69. Chang H, Fitzpatrick JM. A technique for accurate magnetic resonance imaging in the presence of field inhomogeneities. *IEEE Trans Med Imaging.* 1992;11(3):319–29.
  70. Jezzard P, Balaban RS. Correction for geometric distortion in echo planar images from B0 field variations. *Magn Reson Med.* 1995;34(1):65–73.
  71. Baldwin LN, Wachowicz K, Fallone BG. A two-step scheme for distortion rectification of magnetic resonance images. *Med Phys.* 2009;36(9):3917–26.
  72. Eilertsen K, et al. A simulation of MRI based dose calculations on the basis of radiotherapy planning CT images. *Acta Oncol.* 2008;47(7):1294–302.
  73. Kim J, et al. Dosimetric evaluation of synthetic CT relative to bulk density assignment-based magnetic resonance-only approaches for prostate radiotherapy. *Radiat Oncol.* 2015;10(1):239.
  74. Kim J, et al. Implementation of a novel algorithm for generating synthetic CT images from magnetic resonance imaging data sets for prostate cancer radiation therapy. *Int J Radiat Oncol Biol Phys.* 2015;91(1):39–47.
  75. Siverson C, et al. Technical note: MRI only prostate radiotherapy planning using the statistical decomposition algorithm. *Med Phys.* 2015;42(10):6090–7.
  76. Liu L, et al. A female pelvic bone shape model for air/bone separation in support of synthetic CT generation for radiation therapy. *Phys Med Biol.* 2016;61(1):169–82.
  77. Köhler M, et al. MR-only simulation for radiotherapy planning. *Philips White Paper.* 2015.
  78. Persson E, et al. MR-OPERA: a multicenter/multivendor validation of magnetic resonance imaging-only prostate treatment planning using synthetic computed tomography images. *Int J Radiat Oncol Biol Phys.* 2017;99(3):692–700.
  79. Korhonen J, et al. Feasibility of MRI-based reference images for image-guided radiotherapy of the pelvis with either cone-beam computed tomography or planar localization images. *Acta Oncol.* 2015;54(6):889–95.
  80. Kishan AU, et al. Pelvic nodal dosing with registration to the prostate: implications for high-risk prostate cancer patients receiving stereotactic body radiation therapy. *Int J Radiat Oncol Biol Phys.* 2015;91(4):832–9.
  81. Kopp RW, et al. VMAT vs. 7-field-IMRT: assessing the dosimetric parameters of prostate cancer treatment with a 292-patient sample. *Med Dosim.* 2011;36(4):365–72.
  82. Seppala J, et al. Dosimetric comparison and evaluation of 4 stereotactic body radiotherapy techniques for the treatment of prostate cancer. *Technol Cancer Res Treat.* 2017;16(2):238–45.
  83. Wong C, Diamond KR. Optimization of Eclipse Radpiarc's normal tissue objective to determine a standard setting for use in post-prostatectomy radiotherapy treatment planning. *J Med Imag Radiat Sci.* 2013;44(3):158.
  84. Pucar D, et al. Clinically significant prostate cancer local recurrence after radiation therapy occurs at the site of primary tumor: magnetic resonance imaging and step-section pathology evidence. *Int J Radiat Oncol Biol Phys.* 2007;69(1):62–9.
  85. Arrayeh E, et al. Does local recurrence of prostate cancer after radiation therapy occur at the site of primary tumor? Results of a longitudinal MRI and MRSI study. *Int J Radiat Oncol Biol Phys.* 2012;82(5):e787–93.
  86. Aluwini S, et al. Stereotactic body radiotherapy with a focal boost to the MRI-visible tumor as monotherapy for low- and intermediate-risk prostate cancer: early results. *Radiat Oncol.* 2013;8:84.
  87. Groenendaal G, et al. Simultaneous MRI diffusion and perfusion imaging for tumor delineation in prostate cancer patients. *Radiother Oncol.* 2010;95(2):185–90.
  88. Groenendaal G, et al. Validation of functional imaging with pathology for tumor delineation in the prostate. *Radiother Oncol.* 2010;94(2):145–50.
  89. Langer DL, et al. Prostate tissue composition and MR measurements: investigating the relationships between ADC, T2, K(trans), v(e), and corresponding histologic features. *Radiology.* 2010;255(2):485–94.
  90. Zelhof B, et al. Correlation of diffusion-weighted magnetic resonance data with cellularity in prostate cancer. *BJU Int.* 2009;103(7):883–8.
  91. Gibbs P, et al. Correlation of ADC and T2 measurements with cell density in prostate cancer at 3.0 Tesla. *Invest Radiol.* 2009;44(9):572–6.
  92. Wang XZ, et al. Diffusion-weighted imaging of prostate cancer: correlation between apparent diffusion coefficient values and tumor proliferation. *J Magn Reson Imaging.* 2009;29(6):1360–6.
  93. Borren A, et al. Accurate prostate tumour detection with multiparametric magnetic resonance imaging: dependence on histological properties. *Acta Oncol.* 2014;53(1):88–95.



94. Liu X, et al. Prostate cancer segmentation with simultaneous estimation of Markov random field parameters and class. *IEEE Trans Med Imaging*. 2009;28(6):906–15.
95. Langer DL, et al. Prostate cancer detection with multi-parametric MRI: logistic regression analysis of quantitative T2, diffusion-weighted imaging, and dynamic contrast-enhanced MRI. *J Magn Reson Imaging*. 2009;30(2):327–34.
96. Groenendaal G, et al. Pathologic validation of a model based on diffusion-weighted imaging and dynamic contrast-enhanced magnetic resonance imaging for tumor delineation in the prostate peripheral zone. *Int J Radiat Oncol Biol Phys*. 2012;82(3):e537–44.
97. Viswanath SE, et al. Central gland and peripheral zone prostate tumors have significantly different quantitative imaging signatures on 3 Tesla endorectal, in vivo T2-weighted MR imagery. *J Magn Reson Imaging*. 2012;36(1):213–24.
98. Dinh CV, et al. Multicenter validation of prostate tumor localization using multiparametric MRI and prior knowledge. *Med Phys*. 2017;44(3):949–61.
99. Qi P, et al. Offline multiple adaptive planning strategy for concurrent irradiation of the prostate and pelvic lymph nodes. *Med Phys*. 2014;41(2):021704.
100. Chen LN, et al. Stereotactic body radiation therapy (SBRT) for clinically localized prostate cancer: The Georgetown University experience. *Radiat Oncol*. 2013;8:58.
101. Feng Y, et al. Direct aperture deformation: an interfraction image guidance strategy. *Med Phys*. 2006;33(12):4490–8.
102. Court LE, et al. Automatic online adaptive radiation therapy techniques for targets with significant shape change: a feasibility study. *Phys Med Biol*. 2006;51(10):2493–501.
103. Fu W, et al. A cone beam CT-guided online plan modification technique to correct interfractional anatomic changes for prostate cancer IMRT treatment. *Phys Med Biol*. 2009;54(6):1691–703.
104. Mohan R, et al. Use of deformed intensity distributions for on-line modification of image-guided IMRT to account for interfractional anatomic changes. *Int J Radiat Oncol Biol Phys*. 2005;61(4):1258–66.
105. Ahunbay EE, et al. An on-line replanning scheme for interfractional variations. *Med Phys*. 2008;35(8):3607–15.
106. Acharya S, et al. Online magnetic resonance image guided adaptive radiation therapy: first clinical applications. *Int J Radiat Oncol Biol Phys*. 2016;94(2):394–403.